Dose reconstruction in deforming lung anatomy: Dose grid size effects and clinical implications

Mihaela Rosu,[a] Indrin J. Chetty, James M. Balter, Marc L. Kessler, Daniel L. McShan, and Randall K. Ten Haken
Department of Radiation Oncology, The University of Michigan, Ann Arbor, Michigan 48109-0010

(Received 12 December 2004; revised 13 May 2005; accepted for publication 17 May 2005; published 18 July 2005)

In this study we investigated the accumulation of dose to a deforming anatomy (such as lung) based on voxel tracking and by using time weighting factors derived from a breathing probability distribution function (p.d.f.). A mutual information registration scheme (using thin-plate spline warping) provided a transformation that allows the tracking of points between exhale and inhale treatment planning datasets (and/or intermediate state scans). The dose distributions were computed at the same resolution on each dataset using the Dose Planning Method (DPM) Monte Carlo code. Two accumulation/interpolation approaches were assessed. The first maps exhale dose grid points onto the inhale scan, estimates the doses at the "tracked" locations by trilinear interpolation and scores the accumulated doses (via the p.d.f.) on the original exhale data set. In the second approach, the "volume" associated with each exhale dose grid point (exhale dose voxel) is first subdivided into octants, the center of each octant is mapped to locations on the inhale dose grid and doses are estimated by trilinear interpolation. The octant doses are then averaged to form the inhale voxel dose and scored at the original exhale dose grid point location. Differences between the interpolation schemes are voxel size and tissue density dependent, but in general appear primarily only in regions with steep dose gradients (e.g., penumbra). Their magnitude (small regions of few percent differences) is less than the alterations in dose due to positional and shape changes from breathing in the first place. Thus, for sufficiently small dose grid point spacing, and relative to organ motion and deformation, differences due solely to the interpolation are unlikely to result in clinically significant differences to volume-based evaluation metrics such as mean lung dose (MLD) and tumor equivalent uniform dose (gEUD). The overall effects of deformation vary among patients. They depend on the tumor location, field size, volume expansion, tissue heterogeneity, and direction of tumor displacement with respect to the beam, and are more likely to have an impact on serial organs (such as esophagus), rather than on large parallel organs (such as lung). [DOI: 10.1118/1.1949749]

Key words: organ deformation, 4D treatment planning, grid size, dose calculation

I. INTRODUCTION

Motion and deformation induced in human tissue by ventilatory motion can be a major issue in radiation therapy as the standard treatment planning is usually based on a single computed tomography (CT) scan (and hence one instance of the patient's anatomy). Even if the planning CT images are free of motion artifacts[1] the interfraction movement that occurs due to physiological processes within time scales shorter than the delivery of one treatment fraction leads to differences between the planned and delivered dose distributions during a fractionated treatment regimen.[2,3] Due to the influence of these differences on tumors and normal tissues, the tumor control probabilities (TCPs) and normal tissue complication probabilities (NTCPs) are likely to be impacted in the face of organ motion.[4] Moreover, as the recent advances in radiation therapy provide improved target delineation and dose calculation methods, dose distributions are often designed to conform more closely to the targets and the uncertainties associated with organ motion become more apparent. This may limit the success of the conformal radiotherapy thereby leading to local control failure and/or normal tissue complications. It is thus not only desirable, but also necessary to generate, prior to treatment, dose distributions that include the effects of the treatment geometric uncertainties by using the time-varying anatomical information in order to reduce the planning target volume [PTV (Ref. 5)] margins.[6]

The development of methods for incorporating the effect of geometric uncertainties in the dose distribution has been the subject of significant research effort in the past years. An early approach to evaluate the consequences of organ motion on delivered doses was the convolution[2,3,7–12] of the static dose distribution that would result without motion with a kernel that describes the motion characteristics.[2] The inherent assumptions of this method—rigid body anatomy and invariance of the dose distribution under small displacements—limit its usefulness. With the emergence of Monte Carlo as a tool for dose calculation, dose convolution evolved to fluence convolution[13,14] which correctly models the changes in doses due to tissue density variation, while still assuming rigid body motion. Although fluence convolution provides useful information regarding alterations in *tar-*

get coverage in organs that undergo anatomical deformations,[15] dose calculation for the surrounding normal tissues based upon a rigid organ model remains questionable. Consequently there is a need for deformable patient models in regions such as the lung.

A required step toward the estimation of the doses in a deforming anatomy is to establish a correlation between voxels from various representations of the anatomy during radiation delivery. This correlation makes it possible to accumulate dose on a single system of coordinates (e.g., the planning CT data set) for plan evaluation. Research continues into the use of image registration techniques to provide nonrigid body voxel mapping between CT's acquired over various segments of the ventilatory cycle, such as those that incorporate spline transformation models[16–18] and mutual information[19,20] as similarity criterion. Several studies have already investigated the effect of organ deformation on cumulative doses delivered by high energy photon beams in liver[21] and prostate[22] and by heavy-ion therapy in lung.[23] In these studies, the dose grid points from the planning CT are mapped on various breathing phase CT's; the doses at the tracked grid point locations are assumed to be the estimators of the doses received by the planning grid point at a given respiratory phase. However, the validity of this assumption has not been yet investigated.

In the present study we report on the implementation of dose reconstruction in a deforming anatomy based on voxel tracking and by using time weighting factors derived from a breathing probability distribution function. We investigate the validity and the clinical implications of our approach, for example, lung cancer treatment plans.

II. METHODS AND MATERIALS

A. Patient data collection

Under a protocol approved by the Internal Review Board at the University of Michigan, data were acquired for six patients diagnosed with inoperable nonsmall cell lung cancer. Four patients (A, B, C, D) had tumors with volume <100 cm^3, apical, midlateral and midmedial, respectively, whereas patients E and F had larger tumors ($150+$cm^3) located inferior and mediastinal. Patient B was different from the other patients in that the tumor was located in the proximity of the esophagus to the extent that in some regions PTV and esophagus overlapped. The center of the mass of the tumor displacements along the three axes and the combined right and left lung volumes at exhale and inhale are compiled in Table I in order to provide the reader with some information regarding the extent of motion underwent by the tumors and lungs.

CT scans were acquired at normal exhale and inhale states during coached voluntary breath hold. Both exhale and inhale scans were obtained sequentially in the same session in order to eliminate any offset between the two data sets due to setup errors. The scans were acquired using a helical CT scanner (CT/I, General Electric, Milwaukee, WI) using a 5 mm aperture and a pitch of 2. For all patients, treatment plans were designed on the exhale data set; the exhale PTV was formed by a uniform 1 cm expansion of the clinical tumor volume (CTV).

TABLE I. The center of the mass of the tumor displacements along the left-right (LR), anterior-posterior (AP), and superior-inferior (SI) directions and the combined right and lung volumes at exhale and inhale. Negative numbers indicate left, anterior and inferior displacements.

	Tumor displacements (cm)			Combined right and left lung volumes (cc)	
Patient	LR	AP	SI	Exhale	Inhale
A	0.2	−0.6	1.3	3813	4650
B	−0.1	−0.3	0.3	4571	5690
C	−0.2	−1.3	0.1	3623	4049
D	0.1	−0.2	−1.0	5385	5852
E	−0.6	0.3	−1.6	5667	6142
F	−0.7	−1.2	−0.3	2884	3798

B. Distorted datasets

In order to be able to build a deformable model of the patient, CT datasets obtained at exhale (reference) and inhale (homologous) needed to be registered. To achieve this, we used a thin-plate transformation model available within our in-house treatment planning system (UMPlan).[16] In brief, control points were placed manually on the reference and homologous image dataset, the homologous points were iteratively manipulated by the Nelder-Mead simplex algorithm and the homologous point configuration that maximizes the mutual information of the two image datasets was selected as the optimal transformation between the two datasets.

This approach had been used previously[24–26] to map, with sufficient degree of accuracy, the liver or the right lung between two CT scans acquired at different breathing phases for the same patient. In the current study we manually placed 46 control points on the reference (exhale) and the homologous (inhale) dataset in order to provide sufficient degrees of freedom. The points were distributed in the whole thorax and were placed on the tumor and lungs surfaces, in the vicinity of bony structures (ribs) and in the interior of the lung, in places that could be easily identified on both scans. Visual inspection of the deformed images for the lung cases showed the process to be quite adequate for planning purposes, but not perfect. This was expected considering that the thin-plate spline transformation only handles the global deformations.[16] Therefore, we replaced the inhale images with an "inhale phantom" created by using the transformation provided by the registration between the real exhale and inhale datasets—the intent here being to avoid the registration bias in the comparisons between the two dose reconstruction methods described below. Figure 1 shows an example of registration exhale and the "inhale phantom," along with the corresponding joint histogram. The histogram axes represent the possible gray scale values in the reference (I_1) and homologous

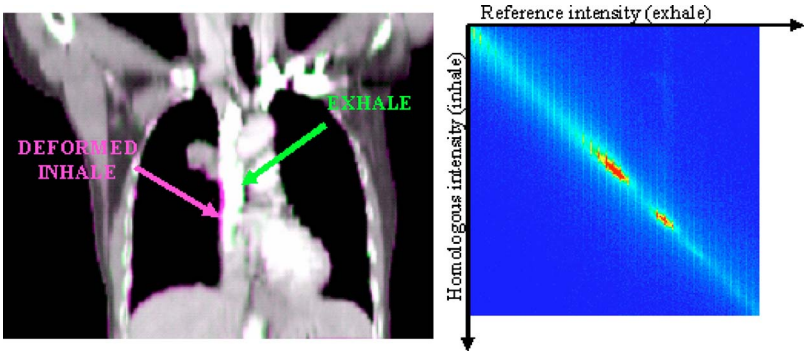

FIG. 1. Thin-plate spline registration (using mutual information as a similarity measure) between the exhale and the "inhale phantom" and the corresponding joint histogram; exhale and deformed inhale images are shown together for comparison. The arrows point toward regions of registration mismatches.

(I_2) images. Each histogram cell is incremented each time a pair $I_1(x,y)/I_2(x,y)$ occurs in the pair of images, where (x,y) are the coordinates of the pixels in each image; thus the histogram is highly focused in perfectly aligned images and the dispersion grows when images are misaligned. The lung tissue densities in the "inhale phantom" were scaled accordingly, so that the total mass of the lung was conserved. For the remaining of the paper the term "inhale" will refer to the "inhale phantom" image dataset.

C. Monte Carlo treatment planning

One major concern in terms of the dose calculation algorithms used in treatment planning is how the tissue heterogeneities are handled, especially in sites such as lung. Thus far, Monte Carlo based algorithms are known to provide the most accurate dose calculation, being limited only by the accuracy of their inputs. At our institution, a virtual source model[27,28] developed for Monte Carlo treatment planning (RT_DPM) using the Dose Planning Method Monte Carlo code system[29] has been integrated within our in-house treatment planning system, UMPlan (University of Michigan, Ann Arbor, MI). RT_DPM was used for all treatment planning calculations in this study. The typical treatment plan beam configuration consisted of conformal 6/15 MV anterior, lateral, and oblique fields, combined with segmental fields (directed from the same angles) to produce a dose distribution of 100±5% within the planning target volume (PTV). The average number of beams per plan was 5 (range 3–7). All plans were normalized to 100% at the isocenter. We used a 2 mm step size, and low energy electron and photon cut-off values of 200 and 10 keV, respectively. For each treatment plan, approximately one billion histories per field were simulated, resulting in 1-σ statistics of better than 1.0% on average within the PTV. Statistical uncertainties for the normal lung tissue, generally located in the low dose region, were typically between 1% and 5.0%, however, volume indices, such as MLD and NTCP are relatively insensitive to even larger point dose uncertainties. The statistical uncertainty in the irradiated region varies approximately as the square root of dose.

The conformal plans (beam arrangement and monitor units) initially designed on the reference dataset (i.e., exhale) were also used for the calculation of the dose distribution on the inhale dataset at the same dose grid resolution. The dose grid size, in all dimensions, ranged from 3.5 mm to 10 mm for the purpose of assessing the grid size effects on the interpolation methods proposed for dose reconstruction (as described in next section).

In addition to comparing the results from the two interpolation schemes on the deformed inhale doses for various grid sizes, we compared the dose calculated on the static exhale dataset with the deformed dose from the inhale datasets, as well as with the cumulative doses, using a grid size of 3.5 mm (in order to minimize the grid size effects).

DVHs for the uninvolved lung (i.e., both lungs minus tumor) served as input for the calculation of the mean lung dose (MLD), and the gEUD (Ref. 30) to tumor was evaluated using an a parameter value of -10, which assumes a moderately aggressive tumor.

D. Dose reconstruction

The basic idea for dose reconstruction was to track dose grid voxels between exhale and inhale using the transformation provided by the registration technique, to obtain an estimate of the dose received at inhale by each exhale voxel and to accumulate this dose back onto the exhale voxel.

In Monte Carlo based calculation algorithms, the dose at each grid point is the average energy deposited into a cubical volume (voxel) centered at the grid point. The simplest estimate of the dose received by the exhale voxel at inhale (which we will call Method 1, a direct approximation) was obtained by mapping the center of the exhale voxel onto the inhale dose grid and by computing the dose at the tracked location by trilinear interpolation of the doses at the closest neighboring dose grid points as shown in Fig. 2(a) (note that only the two-dimensional case is shown for clarity). If there is no voxel expansion at inhale (dashed square), the dose at the tracked center is still likely representative of the energy deposited in the voxel transposed from exhale. However, in the event that after transposition, the exhale voxel expands across several inhale grid points voxels which happen to fall in the high dose gradient regions, the dose at the tracked exhale voxel center may no longer be representative of the energy deposited in the expanded voxel, as there are inhale grid points falling into the expanded voxel that are not accounted for [such as grid points e and f in Fig. 2(a)]. We have therefore refined the interpolation method (Method 2, a refined approximation) as depicted in Fig. 2(b): the volume

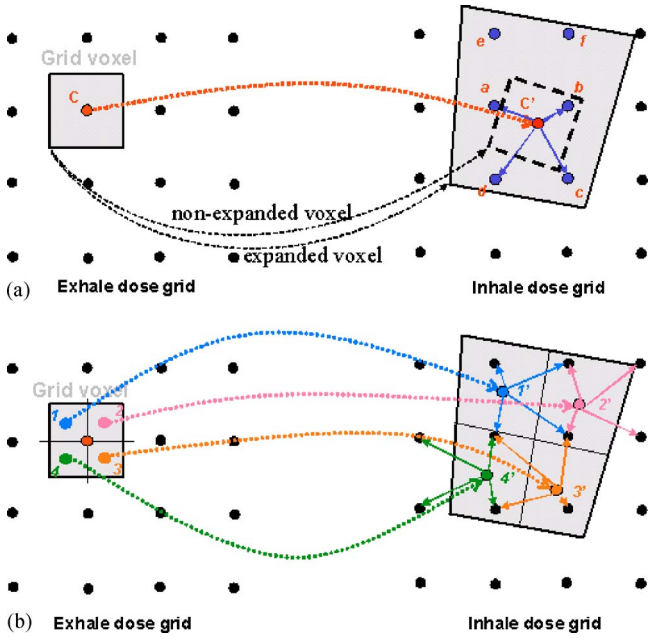

FIG. 2. Two interpolation approaches for estimating the dose received at inhale by each exhale voxel (only the two-dimensional case is shown for clarity): (a) Method 1, direct approximation, the center C of the exhale voxel is mapped at location C′ onto the inhale dose grid and the dose at C′ is estimated by the trilinear interpolation of the doses at the closest neighboring dose grid points *a*, *b*, *c*, *d*. If the exhale voxel expands at inhale, inhale dose grid points such as *e* and *f* that fall into the inhale voxel are not accounted for when dose at C′ is calculated by trilinear interpolation; (b) Method 2, refined approximation, the volume associated with each exhale voxel is first sub-divided into octants, the center of each octant (1,2,3,4) is mapped to locations on the inhale dose grid (1′,2′,3′,4′), doses at the tracked locations are estimated by trilinear interpolation and their average value is scored at the original exhale dose grid point location.

associated with each exhale voxel is first subdivided into octants, the center of each octant is mapped to locations on the inhale dose grid, doses at the tracked locations are estimated by trilinear interpolation, and their average values are scored at the original exhale dose grid point locations.

Accumulation of doses in the deforming dataset was performed by applying time weighting factors representing the relative amount of time spent at a particular breathing phase derived from a breathing probability distribution function,

$$D_{\mathrm{rec}}(i) = \sum_k w_k \cdot D_k(i), \tag{1}$$

where $D_{\mathrm{rec}}(i)$ is the cumulative dose in the exhale voxel i, k the breathing phase, $D_k(i)$ the dose received by exhale voxel i at the breathing phase k, w_k the time weighting coefficient at breathing stage k. As for these investigations, where only the exhale and inhale breathing phases were used, weighting factors of $w_1=70\%$ and $w_2=30\%$ were assigned to be representative of the relative times spent at those two positions, respectively. These weighting coefficients were derived based on the breathing function originally proposed by Lujan *et al.*[2] and shown to be a good approximation for many patients.[31,32]

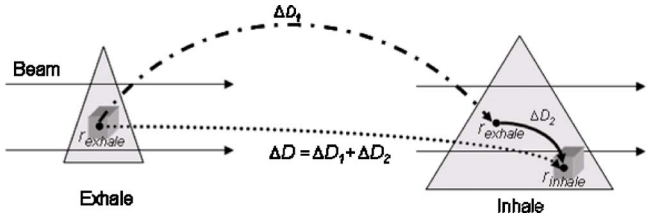

FIG. 3. The overall change in dose at inhale from exhale ΔD can be decomposed in a change in dose ΔD_1 at a point in space due to patient shape and tissue density changes and a change in dose ΔD_2 due to displacement with respect to the beam.

E. Decomposition of inhale doses

In order to better understand the differences between the reconstructed dose that accounts for the motion/deformation effects [which inherently include patient shape (e.g., skin surface) and tissue density changes] induced by ventilation and the original dose distribution planned on the exhale scan, we first analyzed the changes in the inhale dose from the exhale dose. To this end, we decomposed the changes in inhale dose (ΔD) into two components as follows (Fig. 3): for an exhale voxel centered at r_{exhale} in some arbitrary reference system that moves to r_{inhale} in the same reference frame, a change in dose ΔD_1 at a point in space due to changes in patient shape and tissue density alterations, and a change in dose ΔD_2 due to the voxel displacement with respect to the beam due to translational motion and/or deformation.

III. RESULTS

A. Grid size effects

For a given grid size, the dose difference displays between the inhale dose distributions (scored on the exhale planning dataset) as predicted by the two interpolation approaches described above reveal differences in the penumbral region, as it can be seen in the example shown in Fig. 4(a) (here the calculation grid size was 5 mm). The magnitude of the differences between Methods 1 and 2 is influenced by the choice of grid size, increasing from 2% to 6% as the grid size increases from 3.5 mm to 10 mm. These differences occur because the direct approximation (Method 1) does not account for tracked points between inhale and exhale occurring in the high dose gradient region. The profile extracted along the yellow line [Fig. 4(b)] shows that differences tend to have larger magnitude in the higher density tissue (B) due to sharper penumbral slope. Similar magnitude differences between the two interpolation schemes were found for the other five patients involved in this study.

While the differences between the two interpolation schemes are only few percent for any given grid size, the differences between calculations performed using a given interpolation scheme but increasing grid size reveal larger differences. They occur because as the grid size increases, the interpolation tends to underestimate the dose in the upper shoulder and overestimate the dose in the lower shoulder of the profiles.[33] These changes are reflected in the dose volume

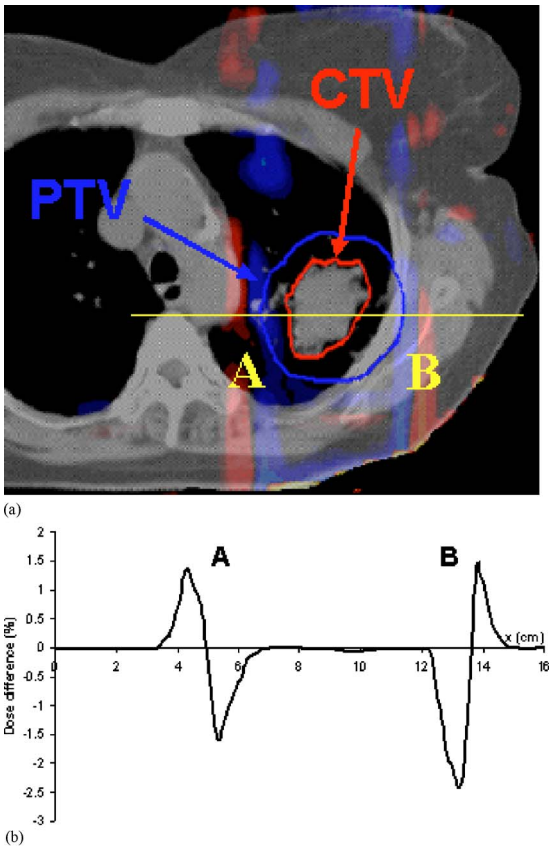

FIG. 4. (a) Dose difference display map between inhale dose distributions mapped back on the exhale dataset as predicted by Method 2 and Method 1 for a 5 mm dose grid calculation (positive/negative differences are indicated in red/blue); (b) Dose profile extracted along the line AB shown in (a).

histograms (DVHs) as shown in Fig. 5 for the ipsilateral lung of Patient A. The use of a larger grid size (10 mm vs 3.5 mm) shows an increase and decrease in the low dose and high dose components of the DVH, respectively.

Table II shows a summary of various treatment metrics used to assess the inhale doses mapped back on the exhale dataset for tumor and normal lung for the 3.5 mm, 5 mm, and 10 mm calculation grids and for both interpolation methods proposed for inhale dose scoring on the planning data set, whereas Table III shows similar data for the esophagus NTCPs for Patient B.

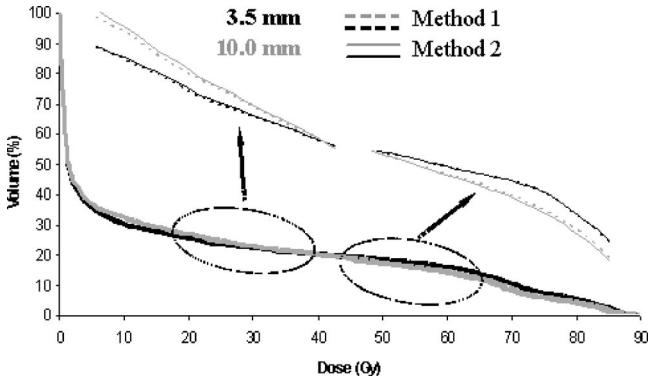

FIG. 5. DVHs for the ipsilateral lung for one of the patients: black lines for 3.5 grid size, gray lines for 10.0 mm grid size, dashed lines for dose estimated by Method 1, solid lines for dose estimated by Method 2.

B. Impact of the breathing induced motion/deformation on the inhale dose

Deviations in doses at inhale from the planning exhale calculations were analyzed for all patients as described in Sec. II E. Figures 6(a)–6(c) show an example of this type of analysis for Patient A. Figure 6(a) shows changes in doses at each point in space created by tissue density and patient shape changes. In Fig. 6(b) hot/cold spots are created in regions that move in/out of the radiation field and their magnitude becomes larger as the displacement gets larger (in this case, the superior and inferior hot/cold spots have larger magnitude than those in the anterior/posterior direction). The overall changes in doses at inhale are large [on the order of 30% as shown for Patient A in Fig. 6(c)] and are primarily due to voxel displacements with respect to the beams. The changes in patient shape and tissue densities on one hand and the displacement with respect to the beam on the other hand may have competing effects as it can be seen in the dashed circle area in Fig. 6 [parts of the hot/cold spots in Fig. 6(a) are canceled out by parts of the cold/hot spots from Fig. 6(b)].

Differences in the doses received by exhale voxels at the inhale versus the exhale phases are reflected in the DVHs, as shown in Fig. 7 for Patient A. The inhale differential CTV DVH (gray line) indicates an overall shift in target coverage toward lower doses compared to the exhale one (black line), including a decrease in the minimum dose to tumor from 79.0 Gy to 75.0 Gy (at 84.0 Gy prescription dose to the isocenter). For this patient most of the tumor underdosage is due to motion. However, this is not always the case. For patient C for example, the underdosage comes mostly from tissue density and shape changes, as shown in Figs. 8(a)–8(c); the minimum dose to tumor dropped from 93.1 Gy to 92.2 Gy at 98.0 Gy prescription dose.

Hot and cold spots of 20%–30% magnitude in steep dose gradient regions surrounding the PTV were found for the other patients as well. They led to increased normal tissue toxicity for Patients A, B, C, and E and decreased toxicity for Patients D and F (Table IV).

C. Impact of the breathing induced motion/deformation on the cumulative dose

While the changes in doses received at inhale compared to exhale are quite significant, the impact of the inhale dose distribution on the cumulative dose is diminished by the fact that its corresponding weighting factor is 30% as it can be seen in Fig. 9(a) for Patient A. As a result, the tumor coverage for well designed PTVs remains almost unaltered and so does the tumors gEUD. The deviations in the ipsilateral lung DVH are also smaller for the same reason and the effect on the total normal lung DHV is even smaller since lungs are parallel organs of large volume. Similar results were found for all patients involved in the study and a summary of the

TABLE II. Summary of the inhale gEUDs (Gy) and MLDs (Gy) for the 3.5 mm, 5 mm, and 10 mm grid size when either Method 1 or Method 2 is used for interpolation.

	Method 1						Method 2					
	Grid size (mm)						Grid size (mm)					
	3.5		5		10		3.5		5		10	
Patient	gEUD	MLD	gEUD	MLD	gEUD	MLD	gEUD	MLD	gEUD	MLD	gEUD	MLD
A	82.9	8.1	82.9	8.1	82.8	8.0	82.9	8.1	82.9	8.1	82.8	8.0
B	97.9	4.0	98.0	4.0	97.4	4.0	97.9	4.0	98.0	4.0	97.5	3.7
C	94.9	13.8	94.9	13.7	94.7	13.7	94.9	13.7	95.0	13.7	94.5	13.7
D	88.6	10.8	88.6	10.8	89.8	10.8	89.9	10.8	88.8	10.8	88.8	10.8
E	65.7	8.2	65.1	8.2	64.3	8.2	65.6	8.2	64.9	8.2	63.2	8.1
F	72.3	14.5	72.2	14.5	71.8	14.5	72.3	14.5	72.2	14.5	71.8	14.6

MLD doses received by the normal lung at the planning stage (exhale), at inhale and in the cumulative doses are shown in Table IV. The comparison between the doses reconstructed using both accumulation methods proposed shows (for this patient as well as for all patients in this study) differences less than 0.5% [Fig. 9(b)].

For Patient B, a 5% hot spot emerged in esophagus in the cumulative dose increasing its estimated probability of toxicity from 4.7% to 5.5%. Although the maximum doses were nearly the same in both plans, the amount of dose in the intermediate dose range led to a clear separation between DVHs in this region as shown in Fig. 10.

IV. DISCUSSION

A. Grid size effects

While differences between the two methods proposed for scoring dose on the planning data set exist, their magnitude (small regions of few percent) is less than the changes in dose induced by positional and shape changes from ventilation and than the errors due to an increasing dose calculation grid. Therefore, differences due solely to the interpolation approach used to map doses from a given dataset back on the planning dataset (exhale in our study) do not result in clinically significant alterations in volume-based evaluation metrics such as mean lung dose, esophagus NTCP and tumor equivalent uniform dose (gEUD).

The choice of the grid size for dose calculation did not have an impact on tumor coverage and mean lung doses either, but led to erroneous estimates of the esophagus NTCPs for Patient B. This is because esophagus is a serial organ and thus it is sensitive to local changes in doses, as opposed to lungs for example for which is the mean dose that describes the sensitivity to radiation.

TABLE III. Summary of the inhale esophagus NTCPs (%) for Patient B for the 3.5 mm, 5 mm, and 10 mm grid size when either Method 1 or Method 2 is used for interpolation.

Method 1 Grid size (mm)			Method 2 Grid size (mm)		
3.5	5	10	3.5	5	10
13.4	7.7	2.4	13.1	7.6	2.4

The esophagus NTCP data for Patient B also suggests that the results of Method 2 do not necessarily match the results from Method 1 with a finer grid resolution, the reason being that a larger calculation grid inherits erroneous voxel dose estimation in the first place.

B. Impact of the breathing induced motion/deformation on the cumulative dose

While the number of patients involved in this study is too small to draw general conclusions regarding what the consequences of motion/deformation are, it appears that although motion and deformation do redistribute doses, changes are not clinically significant. For tumors, this is a consequence of a good PTV design. As far as the normal lung tissue is concerned, motion and deformation lead to either increased or decreased lung toxicity at inhale, but the effects on the cumulative dose are small for two reasons: first, the hot/cold spots attributed to motion/deformation that occur at inhale are diminished by the fact that they average out in larger inhale volumes; second, the inhale doses only have a 30% contribution in the cumulative dose.

The situation is different for serial organs. In the example shown in the previous section, Patient B was treated at the maximum prescription dose allowed by an upper 5% limit in the esophagus NTCP for late toxicity. However, the cumulative dose indicated increased probability for esophagitis above the upper bound as a result of motion/deformation.

The development of a method for dose reconstruction in a deforming anatomy, as presented in this work represents just one step toward implementation of 4D treatment planning. Our results indicate that simply tracking dose grid points between various breathing phases is a sufficiently accurate approach, but the calculation grid size needs to be kept small enough so that the interpolation errors are not significant. However, the effects of motion/deformation will need to be assessed for more patients, since the differences observed between the two interpolation methods may be important in

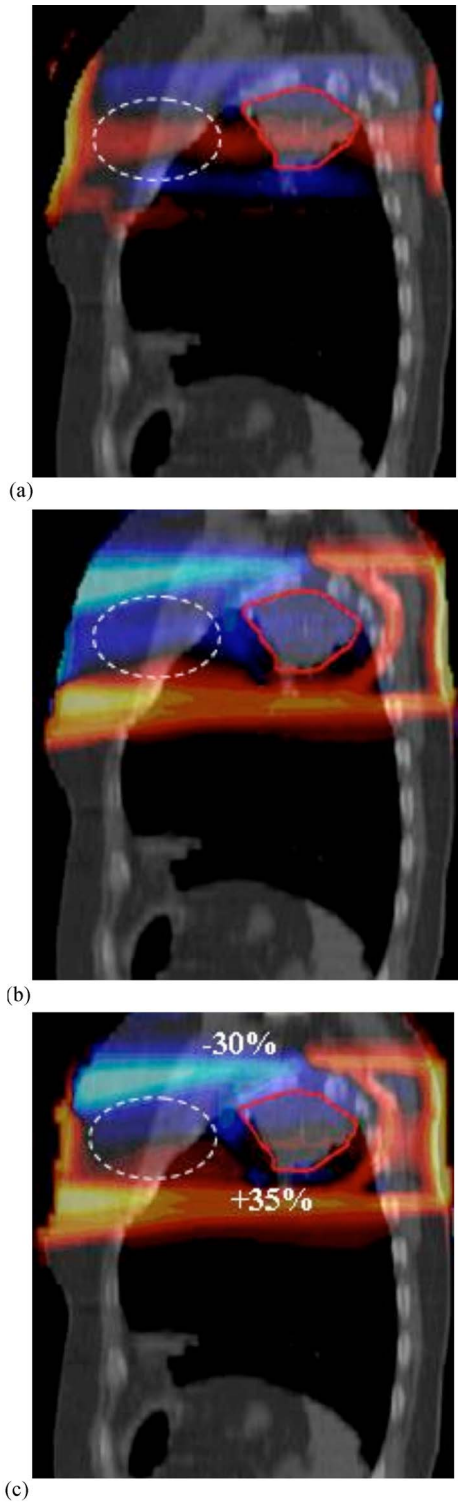

FIG. 6. Patient A. (a) Differences at each point in space between the inhale and the exhale dose distributions; (b) Changes in the inhale voxel doses due to displacements with respect to the beam; (c) Overall changes in the dose received by each exhale voxel at inhale compared to exhale.

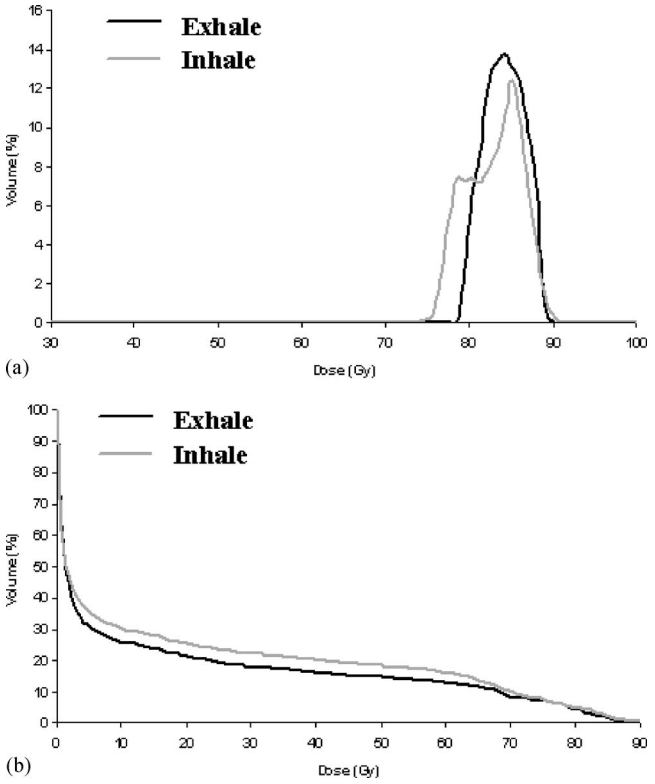

FIG. 7. Dose volume histograms for the patient shown in Fig. 5: (a) direct CTV DVH and (b) cumulative DVH for the ipsilateral lung for exhale (black) and inhale (grey) dose distributions.

some cases. For example, it may be possible for the cold spots in the vicinity of the tumor to lead to important changes in target coverage as the CTV-PTV margin shrinks and the plan becomes more conformal. Also, either the cold or the hot spots may become important if they happen to fall in different neighboring organs instead of canceling out in the same organ or if they fall into a serial organ (such as spine or esophagus) rather than a parallel one.

Also, the registration method used does not account for local deformation and additional investigations are required to assess the possible effects caused by such deformations. In this study we have used only two breathing phases (exhale and inhale) which are believed to be the most representative due to the largest amount of time spent in this states during one breathing cycle, but more work is needed to validate this assumption. The recent developments in 4D imaging techniques will allow for a more detailed analysis in order to estimate the number of intermediate states required to reach convergence in the reconstructed cumulative dose. Also, im-

TABLE IV. Mean lung doses for the exhale, inhale, and reconstructed cumulative dose distributions for the 3.5 mm grid size dose calculations and using Method 1 for dose accumulation.

	Mean lung dose (Gy)		
Patient	Exhale	Inhale	Cumulative
A	7.4	8.1	7.5
B	3.6	4.0	3.7
C	13.5	13.8	13.7
D	11.1	10.8	10.9
E	7.2	8.2	7.5
F	17.0	14.5	16.5

FIG. 8. Patient C. (a) Differences at each point in space between the inhale and the exhale dose distributions; (b) Changes in the inhale voxel doses due to displacements with respect to the beam; (c) Overall changes in the dose received by each exhale voxel at inhale compared to exhale.

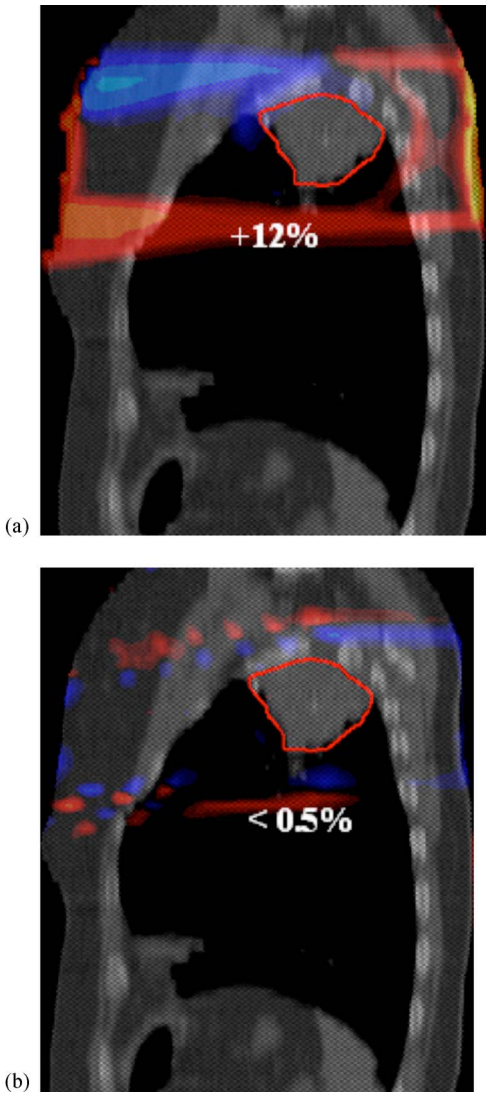

FIG. 9. (a) Dose difference display between the cumulative dose that has 70% contribution from exhale and 30% from inhale and the exhale dose only for Patient A; (b) Dose differences between the reconstructed cumulative doses using refined and direct interpolation schemes (dose estimated by Method 2 minus dose estimated by Method 1).

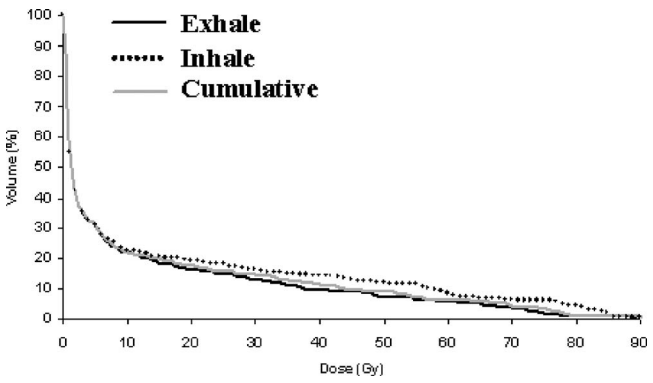

FIG. 10. Cumulative DVH for the esophagus for exhale (solid black), inhale (dotted), and cumulative (solid grey) dose distributions for Patient B.

proved tumor tracking methods will allow for the derivation of the breathing pattern for each patient and time weighting factors could potentially be derived in each case.

In conclusion, we have implemented and investigated two methods for dose reconstruction in the presence of motion and deformation. The differences between the two interpolation approaches appear primarily in steep dose gradient regions. They are voxel size and tissue density dependent. However, the magnitude of these differences is less than the alterations in dose due to positional and shape changes in the first place. The overall changes in the cumulative dose follow

the displacement of voxels with respect to the beam. The overall effects have variability among patients, being dependent on tumor location, field size, tissue heterogeneity, and direction of tumor with respect to the beam. Large parallel organs such as lung are likely to be less sensitive to changes in doses emerging from motion and deformation, while in certain cases these changes may have an impact on serial organs such as esophagus. The method proposed is straightforward and can be easily implemented for any number of intermediate states and breathing patterns.

ACKNOWLEDGMENT

This work was supported by NIH Grant No. P01 CA59872. The authors would like to thank Dan Tatro, CMD, for the help provided with treatment planning.

[a]Electronic mail: mrosu@med.umich.edu

[1]J. M. Balter *et al.*, "Uncertainties in CT-based radiation therapy treatment planning associated with patient breathing," Int. J. Radiat. Oncol., Biol., Phys. **36**, 167–174 (1996).
[2]A. E. Lujan *et al.*, "A method for incorporating organ motion due to breathing into 3D dose calculations," Med. Phys. **26**, 715–720 (1999).
[3]A. E. Lujan *et al.*, "Quantization of setup uncertainties in 3-D dose calculations," Med. Phys. **26**, 2397–2402 (1999).
[4]M. Rosu *et al.*, "Alterations in normal liver doses due to patient motion," Int. J. Radiat. Oncol., Biol., Phys. **57**, 1472–1479 (2003).
[5]International Commission on Radiation Units and Measurements, "ICRU Report 50: Prescribing, recording, and reporting photon beam therapy," Bethesda, MD, 1993.
[6]R. K. Ten Haken *et al.*, "Potential benefits of eliminating planning target volume expansions for patient breathing in the treatment of liver tumors," Int. J. Radiat. Oncol., Biol., Phys. **38**, 613–617 (1997).
[7]J. Leong, "Implementation of random positioning error in computerised radiation treatment planning systems as a result of fractionation," Phys. Med. Biol. **32**, 327–334 (1987).
[8]P. J. Keall *et al.*, "A method to predict the effect of organ motion and set-up variations on treatment plans," Australas. Phys. Eng. Sci. Med. **22**, 48–52 (1999).
[9]S. D. McCarter *et al.*, "Evaluation of the validity of a convolution method for incorporating tumour movement and set-up variations into the radiotherapy treatment planning system," Phys. Med. Biol. **45**, 923–931 (2000).
[10]T. Craig *et al.*, "Limitations of a convolution method for modeling geometric uncertainties in radiation therapy. I. The effect of shift invariance," Med. Phys. **30**, 2001–2011 (2003).
[11]T. Craig *et al.*, "Limitations of a convolution method for modeling geometric uncertainties in radiation therapy. II. The effect of a finite number of fractions," Med. Phys. **30**, 2012–2020 (2003).
[12]A. E. Lujan *et al.*, "A method for incorporating organ motion due to breathing into 3D dose calculations in the liver: Sensitivity to variations in motion," Med. Phys. **30**, 2643–2649 (2003).
[13]W. A. Beckham *et al.*, "A fluence-convolution method to calculate radiation therapy dose distributions that incorporate random set-up error," Phys. Med. Biol. **47**, 715–720 (1999).
[14]I. J. Chetty *et al.*, "A fluence convolution method to account for respiratory motion in three-dimensional dose calculations of the liver: A Monte Carlo study," Med. Phys. **30**, 1776–1780 (2003).
[15]I. J. Chetty *et al.*, "Accounting for center-of-mass target motion using convolution methods in Monte Carlo-based dose calculations of the lung," Med. Phys. **30**, 1776–1780 (2003).
[16]C. R. Meyer *et al.*, "Demonstration of accuracy and clinical versatility of mutual information for automatic multimodality image fusion using affine and thin-plate spline warped geometric deformations," Med. Image Anal **1**, 195–206 (1997).
[17]F. L. Bookstein, "Principal warps: Thin-plate splines and the decomposition of deformations," IEEE Trans. Pattern Anal. Mach. Intell. **11**, 567–585 (1989).
[18]M. Kessler *et al.*, "Deformable image registration using multiresolution b-splines," Med. Phys. **31**, 1792 (2004).
[19]P. A. Viola and W. M. Welles, "Alignment by maximization of mutual information," in Proceedings of the Fifth International Conference on Computer Vision, IEEE95CH35744, 16–23 (1995).
[20]W. M. Welles 3rd *et al.*, "Multi-modal volume registration by maximization of mutual information," Med. Image Anal **1**, 35–51 (1996).
[21]K. K. Brock *et al.*, "Inclusion of organ deformation in dose calculation," Med. Phys. **30**, 290–295 (2003).
[22]B. Schaly *et al.*, "Tracking the dose distribution in radiation therapy by accounting for variable anatomy," Phys. Med. Biol. **49**, 791–805 (2004).
[23]E. Rietzel *et al.*, "4D treatment planning: calculation of voxel doses in the presence of respiratory motion," Med. Phys. **31**, 1751 (2004).
[24]C. Meyer *et al.*, "Method for quantifying volumetric lesion change in liver CT examinations," IEEE Trans. Med. Imaging **22**, 776–781 (2003).
[25]K. K. Brock *et al.*, "Automated generation of a four-dimensional model of the liver using warping and mutual information," Med. Phys. **30**, 1128–1133 (2003).
[26]M. M. Coselmon *et al.*, "Mutual information based CT registration of the lung at exhale and inhale breathing states using thin-plate splines," Med. Phys. **31**, 2942–2948 (2004).
[27]I. J. Chetty *et al.*, "A virtual source model for Monte Carlo modeling of arbitrary intensity distributions," Med. Phys. **27**, 166–172 (2000).
[28]I. J. Chetty *et al.*, "Photon beam relative dose validation of the DPM Monte Carlo code in lung-equivalent media," Med. Phys. **30**, 563–573 (2003).
[29]J. Sempau *et al.*, "DPM, a fast, accurate Monte Carlo code optimized for photon and electron radiotherapy treatment planning calculations," Phys. Med. Biol. **45**, 2263–2291 (2000).
[30]A. Niemierko, "A generalized concept of equivalent uniform dose (gEUD)," Med. Phys. **26**, 1100 (1999).
[31]Y. Seppenwoolde *et al.*, "Precise and real-time measurement of 3D tumor motion in lung due to breathing and heartbeat, measured during radiotherapy" Int. J. Radiat. Oncol., Biol., Phys. **53**, 822–34 (2002).
[32]S. Shimizu *et al.*, "Detection of lung tumor movement in real-time tumor-tracking radiotherapy," Int. J. Radiat. Oncol., Biol., Phys. **51**, 304–310 (2001).
[33]A. Niemierko *et al.*, "The influence of the size of the grid used for dose calculation on the accuracy of dose estimation," Med. Phys. **16**, 239–247 (1989).